Preprint
UCRL-JC-145897

EUVL Mask Blank Repair

A. Barty, P.B. Mirkarimi, D.G. Stearns, D. Sweeney, H.N. Chapman, M. Clift, S. Hector, M. Yi

This article was submitted to
Microlithography 2002, Santa Clara, California, March 3-8, 2002

May 22, 2002

U.S. Department of Energy

Lawrence
Livermore
National
Laboratory

UCRL-JC-145897-Abs-

EUVL mask blank repair

Anton Barty, Paul B. Mirkarimi, Daniel G. Stearns, Don Sweeney, Henry N. Chapman,
Lawrence Livermore National Laboratory
Livermore, CA. 94550

Miles Clift
Sandia National Laboratories
Livermore, CA. 94550

Scott Hector
Motorola DigitalDNA™ Labs
Austin, TX 78721

and

Moonsuk Yi
Lawrence Berkeley National Laboratories
Berkeley, CA, 94720

EUV mask blanks are fabricated by depositing a reflective Mo/Si multilayer film onto super-polished substrates. Small defects in this thin film coating can significantly alter the reflected field and introduce defects in the printed image. Ideally one would want to produce defect-free mask blanks; however, this may be very difficult to achieve in practice. One practical way to increase the yield of mask blanks is to effectively repair multilayer defects, and to this effect we present two complementary defect repair strategies for use on multilayer-coated EUVL mask blanks.

A defect is any area on the mask which causes unwanted variations in EUV dose in the aerial image obtained in a printing tool, and defect repair is correspondingly defined as any strategy that renders a defect unprintable during exposure. The term defect mitigation can be adopted to describe any strategy which renders a critical defect non-critical when printed, and in this regard a non-critical defect is one that does not adversely affect device function.

Defects in the patterned absorber layer consist of regions where metal, typically chrome, is unintentionally added or removed from the pattern leading to errors in the reflected field. There currently exists a mature technology based on ion beam milling and ion beam assisted deposition for repairing defects in the absorber layer of transmission lithography masks, and it is reasonable to expect that these this technology will be extended to the repair of absorber defects in EUVL masks[1]. However, techniques designed for the repair of absorber layers can not be directly applied to the repair of defects in the mask blank, and in particular the multilayer film. In this paper we present for the first time a new technique for the repair of amplitude defects as well as recent results on the repair of phase defects.

Keywords: extreme ultraviolet lithography; mask; reticle; defect; multilayer; printability; cost of ownership.

1 Multilayer defect classification

A problem unique to EUVL is the existence of defects in the reflective multilayer coating applied to mask blanks prior to patterning. A typical EUV multilayer coating consists of 40-60 bilayers of molybdenum and amorphous silicon, with each bilayer consisting of approximately 3nm Mo and 4nm Si. The reflectivity of the multilayer is a

---

[1] T.Liang et.al. "Progress in EUV mask repair using a focussed ion beam" **18(6)** J.Vac.Sci.Ttechnol.B. 3216, 2000.

resonant property of the alternating layer structure formed when the layers interfere constructively; because reflection takes place throughout the bulk of the multilayer any deformation or disruption of the layer structure can become a defect.

For the purpose of this paper we classify multilayer defects into two categories. Defects nucleated towards the start of the multilayer deposition process propagate upwards through the multilayer during deposition as illustrated in Figure 1(a) and are typically nucleated by particles or defects on the substrate prior to coating or by defects introduced during deposition of the first few layers, but may also be caused by random fluctuations in the deposition process. During the multilayer deposition low frequency components of underlying layers are efficiently replicated by overlying layers, thus particles near the base of the substrate result in deformation of the multilayer structure throughout its bulk. The resulting deformation in multilayer structure cases a change in the phase of the reflected field which, if the size of the perturbation exceeds a critical size of approximately 1.5nm in height and 100nm in width, results in a change in the printed image and therefore represents a defect in the multilayer[2]. Because these defects produce a modulation of the phase of reflected field we term these defects 'phase defects'.

By way of contrast defects nucleated near or at the top of the multilayer coating shadow underlying layers and thereby attenuate the reflected field. Such defects, illustrated in Figure 1(b), are either introduced subsequent to multilayer deposition or during deposition of the top layers and can affect the multilayer reflectivity in one of two ways:

(a) if the particle is opaque the incident field does not penetrate the defect and the amplitude of the reflected field is directly reduced; or

(b) the particle can damage the multilayer structure in its vicinity, either during the embedding process or by perturbing the subsequent multilayer growth, reducing the multilayer reflectivity which in turn decreases the amplitude of the reflected field.

Even if the particle does not remain embedded in the coating the damage caused to the multilayer structure itself can act as an amplitude defect because the multilayer structure has been damaged in the region where the particle was located. We therefore classify these defects as 'amplitude defects' because they primarily affect the amplitude of the reflected field.

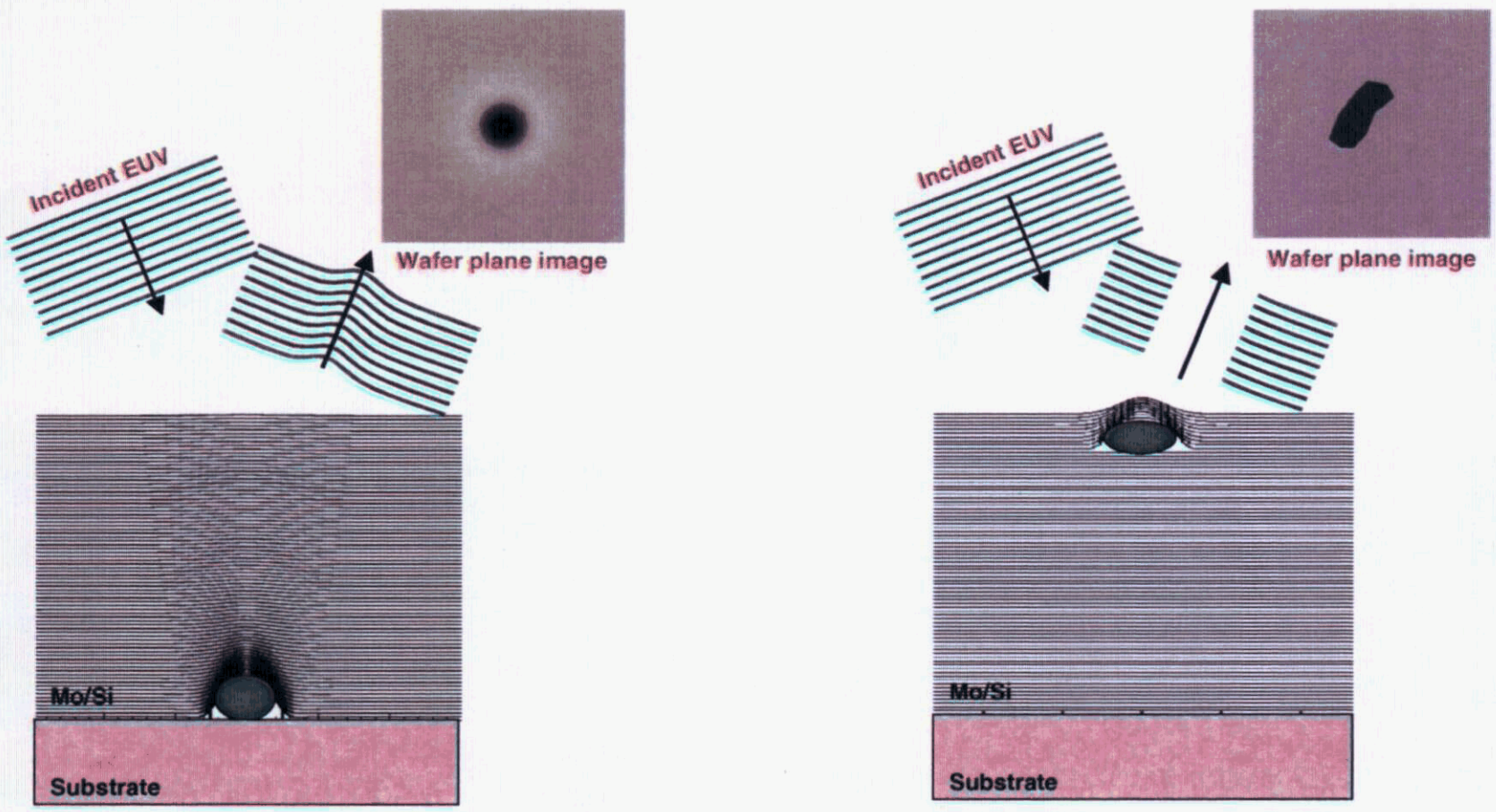

(a) Phase defect nucleated at base of multilayer

(b) Amplitude defect nucleated at the top of the multilayer

Figure 1

Particles located at the base of the film produce a different type of defect to those located at the top of the multilayer stack.

---

[2] E.M.Gullikson, C.Cerjan, D.G.Stearns, P.B.Mirkarimi and D.W.Sweeney; "Practical approach for modeling extreme ultraviolet lithography mask defects" (2002) **20** J.Vac.Sci.Technol.B. 81.

2 Amplitude defect repair

The basic principle of the amplitude repair method is to restore the local reflectivity by removing the particle, if it still exists, and any damaged regions of the multilayer coating. This can be done by physically removing the particle using a focussed ion beam as shown in Figure 2. This process leaves behind a shallow crater in the multilayer, but if done in a properly controlled manner the reflectivity of the repaired region can be restored to nearly defect-free levels and the effect of the defect on the printed image thereby mitigated.

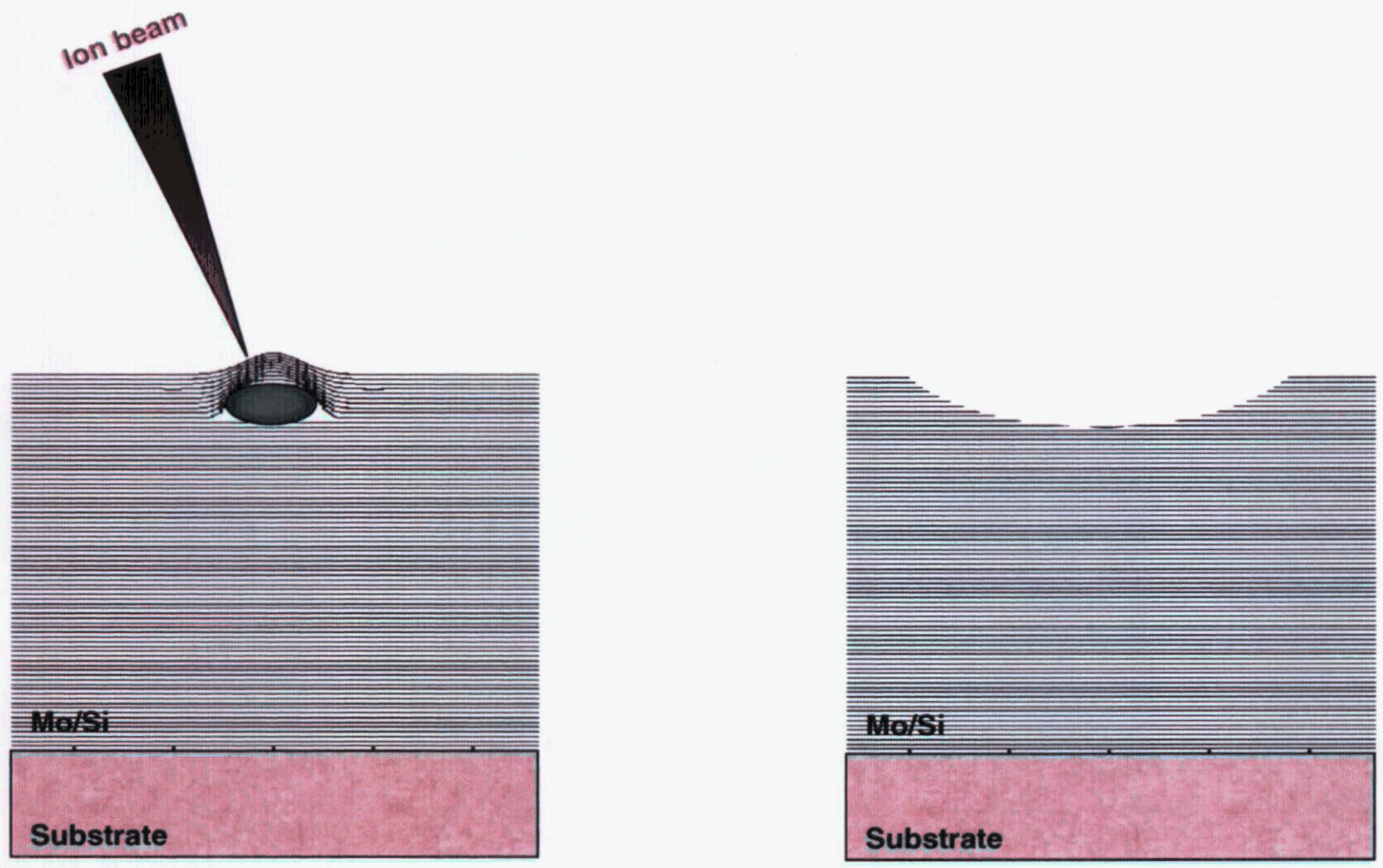

(a) Amplitude defect removal using a focussed ion beam.

(b) Amplitude defect after repair – a small crater remains in the multilayer.

Figure 2

To be effective the repair process must satisfy the constraint that there be no significant variation in contrast in the bright-field intensity of a lithographic image across the repaired area. In practice this means that:

(a) a sufficient number of multilayers must remain after repair for the reflectivity degradation to be negligible,
(b) that any phase shifts introduced by milling out a small region of the reflective surface be sufficiently small that the phase structure of the crater does not itself introduce a defect into the printed image;
(c) that the underlying layers of the multilayer stack remain undamaged so that they can still reflect EUV light; and
(d) that there is no deposition of particles elsewhere on the mask blank resulting from the milling process.

It is relatively easy to control the reflectivity modulation due to layer removal as multilayer reflectivity is a direct function of the number of bilayers in the multilayer stack. For Mo/Si multilayers at 13.4nm the reflectivity reaches approximately 99% of the maximum attainable value by the time there are 40 bilayers; A typical mask blank will have between 50 and 60 bilayer pairs in the multilayer stack, thus removing up to 20 bilayers from a 60-bilayer multilayer will alter the intensity of the reflected field by less than 1% due to layer removal alone. This linking of the number of layers removed with multilayer reflectivity does, however, impose a practical limitation on the depth of defect that can be removed using this technique. Note that there is also an effect on the reflectivity due to exposing different

terminating layers as the top layer of the multilayer which has to be taken into account. The magnitude of this effect is dependent on the composition of the topmost surface layers and will be discussed in more detail below.

The crater profile must be carefully controlled so as to minimise printability of the repaired region in a lithographic tool. The layered structure of a multilayer mirror means that all of the waves must be in phase with respect to each other within the multilayer itself, thus the optical path difference (OPD) for light reflected from a Gaussian-shaped crater is of the form

$$p(\vec{r}) = 2(n-1)he^{-r^2/w^2}$$

where n is the average refractive index of the multilayer, h is the maximum depth of the crater, and ω is the 1/e radius of the crater on the mask. The refractive index of the multilayer is given by the ratio of the wavelengths of light in vacuum (λ) to that in the multilayer, and for a typical near-normal incidence EUV multilayer at λ=13.43nm the multilayer period is 13.80nm giving a value of the refractive index of the multilayer (1-n) = 0.03. That is to say that the refractive index of the multilayer is very nearly the same as for vacuum, thus the phase shift for a given crater depth is just 0.03 times the profile of the crater itself.

Assuming that the crater profile is gentle enough that light is not scattered outside of the pupil the dominant effect of the crater phase structure within the process-window of the lithographic tool is due to defocus, and it can be shown using arguments based on the transport of intensity equation[3] that the maximum contrast C_{max} within the process window of a lithographic tool is proportional to the gradient of the crater and is given by

$$C_{max} = 1.45\frac{(1-n)N}{n(w/\delta)^2}$$

where $\delta=\lambda/2NA_{ent}$ is the spatial resolution of the lithographic tool facing the mask and N is the number of bilayers removed, and we see that craters with gently sloping sides will not print as easily as craters with steep sides. For the removal of 20 bilayers from a Mo/Si multilayer mask we have $C_{min}=0.89\delta^2/\omega^2$, and to ensure that the contrast induced by the repair is less than 1% we must have $\omega>9.45\delta$. In practical terms this means that for a 0.25NA 4x stepper system operating at 13.4nm we need 20 bilayer (130nm) deep repair craters to be 4μm or more in diameter.

To demonstrate this technique we milled craters in multilayers using a low energy (500eV) Ar ion mill. We chose to mill using 500eV Ar ions incident at 50 degrees off normal to minimise penetration of the ions into the multilayer and thus damage to the multilayer structure itself and thereby preserve the reflectivity. Craters of a depth of between 5 and 20 bi-layer thickness (30-130nm deep) were milled in multilayers consisting of 40 bi-periods of Mo/Si deposited on superpolished Si wafers, the reflectivity of which was typically 66% at 13.4nm prior to milling. We milled craters of approximately 2mm diameter due to limitations on the spatial resolution of the ion gun in the sputter Auger system used for these experiments. However one benefit of producing such large craters was that we could obtain measurements of the EUV reflectivity using scanning reflectometers at the Advanced Light Source (ALS) at Lawrence Berkeley Laboratories[4].

An example of one of the deeper craters we have fabricated is shown in Figure 3. Figure 3(a) shows a secondary electron image of a 20 bi-layer deep crater immediately after milling. The alternating light and dark bands are the alternate layers of Molybdenum and Silicon exposed as the top layer during crater manufacture. Figure 3(b) shows a profile of the crater taken using a Zygo white light interferometric microscope (top) and a section through the deepest part of the crater (lower). Note that the vertical scale is greatly exaggerated and that the milled region is 2mm across and 130nm deep, an aspect ratio of approximately 10000:1.

---

[3] M.R.Teague "Image formation in terms of the transport equation" **11** J.Opt.Soc.Am.A. 2019 (1985).

[4] The reflectometer on beamline 6.3.2 at the ALS has a typical spot size of 100x300μm whilst the BL11.3.2 reflectometer has a typical spot size of 3x3μm. E.M.Gullikson, S. Mrowka, and B.B. Kaufmann, "Recent Developments in EUV Reflectometry at the Advanced Light Source," *Emerging Lithographic Technologies V*, SPIE vol. 4343, (2001).

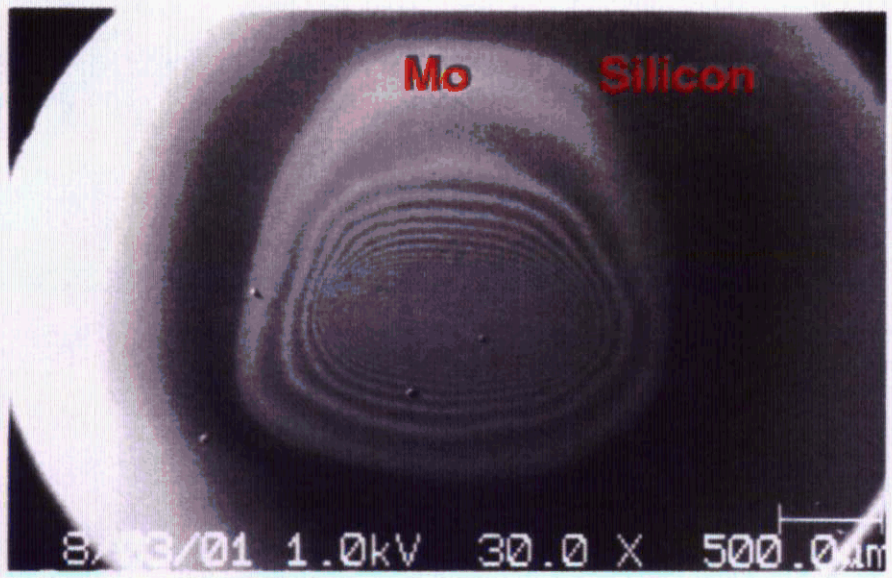

(a)

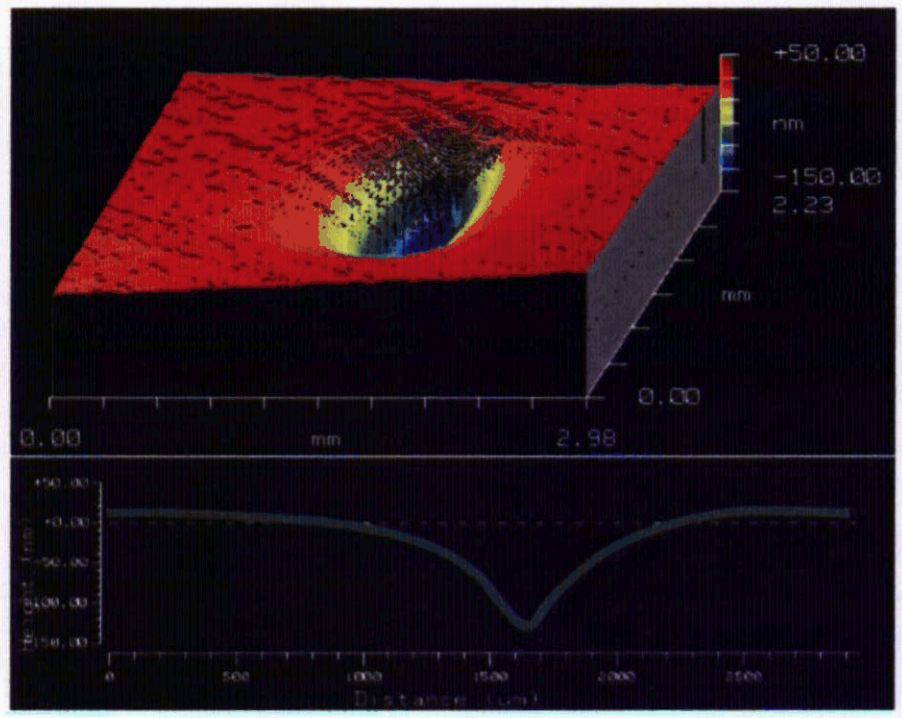

(b)

Figure 3

(a) Secondary electron image of a 20 bi-layer deep crater immediately after milling. The alternating light and dark bands are the alternating layers of Molybdenum and Silicon exposed during the crater manufacture. (b) Profile of the crater taken using a Zygo white light microscope (top) and a section through the deepest part of the crater (lower). Note that the vertical scale is greatly exaggerated – the milled region is 2mm across and 130nm deep, an aspect ratio of approximately 10000:1.

The milled craters were analysed for reflectivity variations at both the beamline 11.3.2 actinic inspection tool and the beamline 6.3.2 reflectometer at the Advanced Light Source in Berkeley (ALS). Results of the high-resolution inspection are shown below in Figure 4 – Figure 4(a) shows a 2D scan of the crater region and Figure 4(b) a horizontal line profile through the deepest part of the crater. Note that the ring structure resulting from alternately exposed layers of Mo and Si are clearly visible, with the regions where the Mo layers are exposed having lower reflectivity than the areas where Si forms the upper layer.

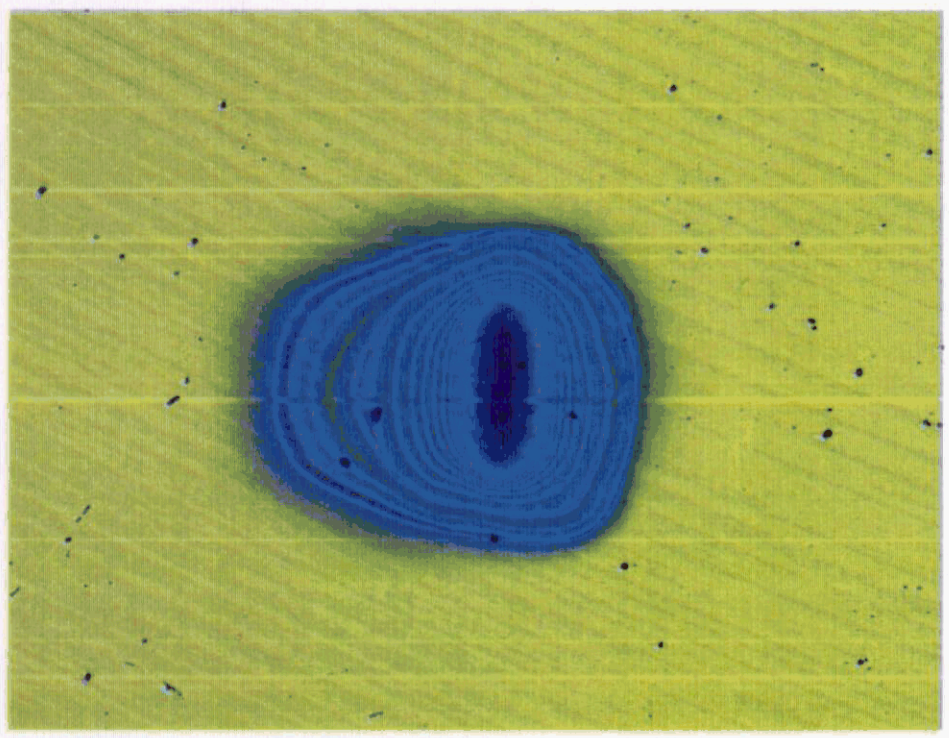

(a)

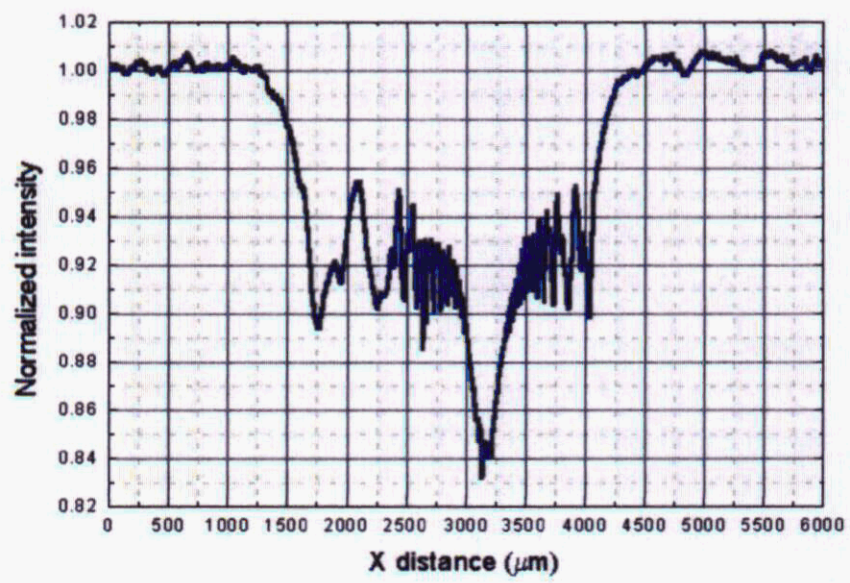

(b)

Figure 4

At wavelength measurements of the EUV reflectivity of the crater shown in Figure 3 above: (a) 2D at-wavelength scan of the crater and (b) horizontal line-out of the reflectivity through the deepest part of the crater. The vertical axis is the reflectivity normalized with respect to the signal outside of the crater and represents the relative reflectivity of the scanned area.

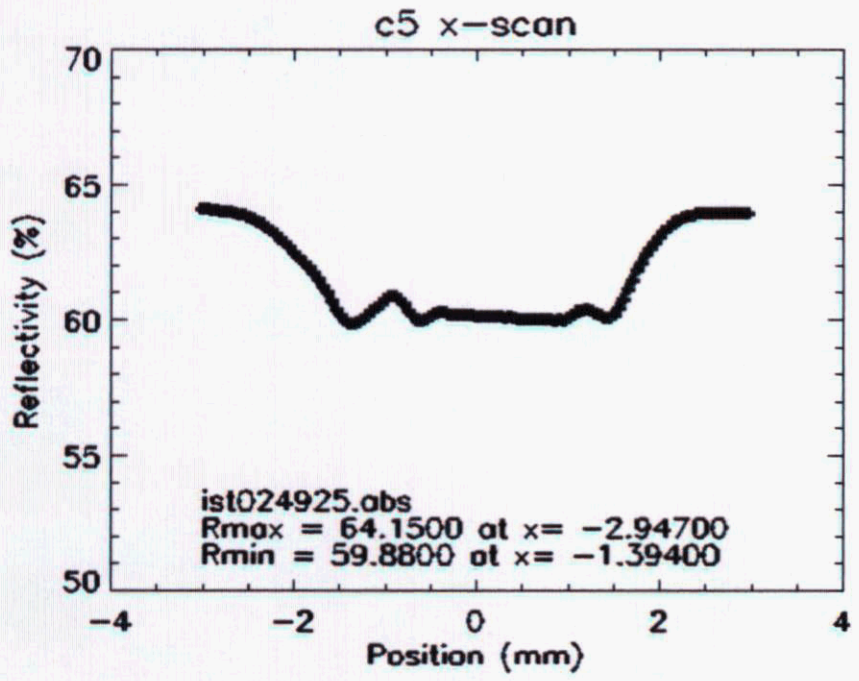

5 bi-layer deep crater

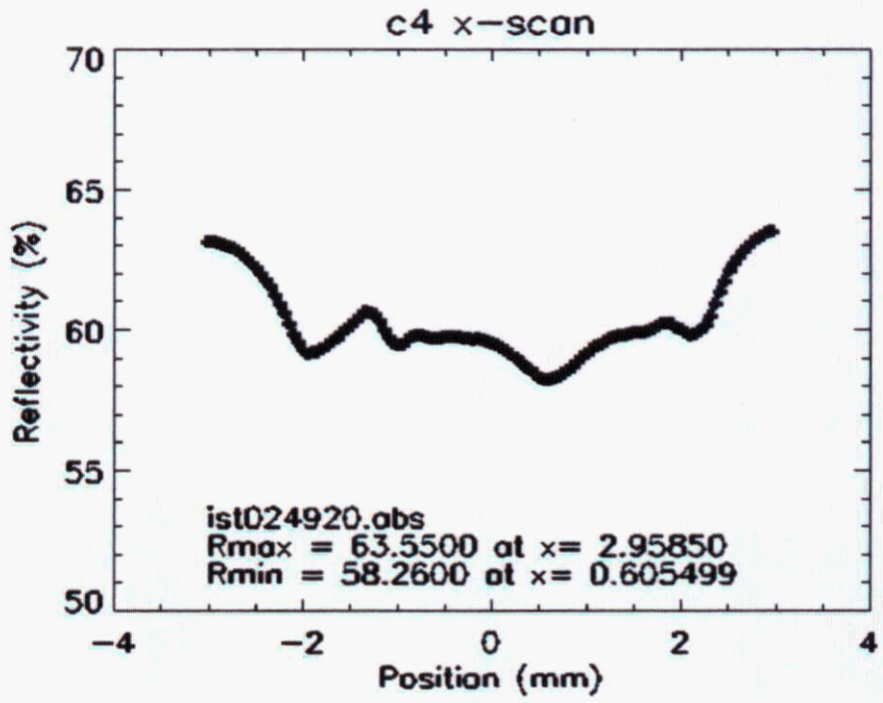

15 bi-layer deep crater

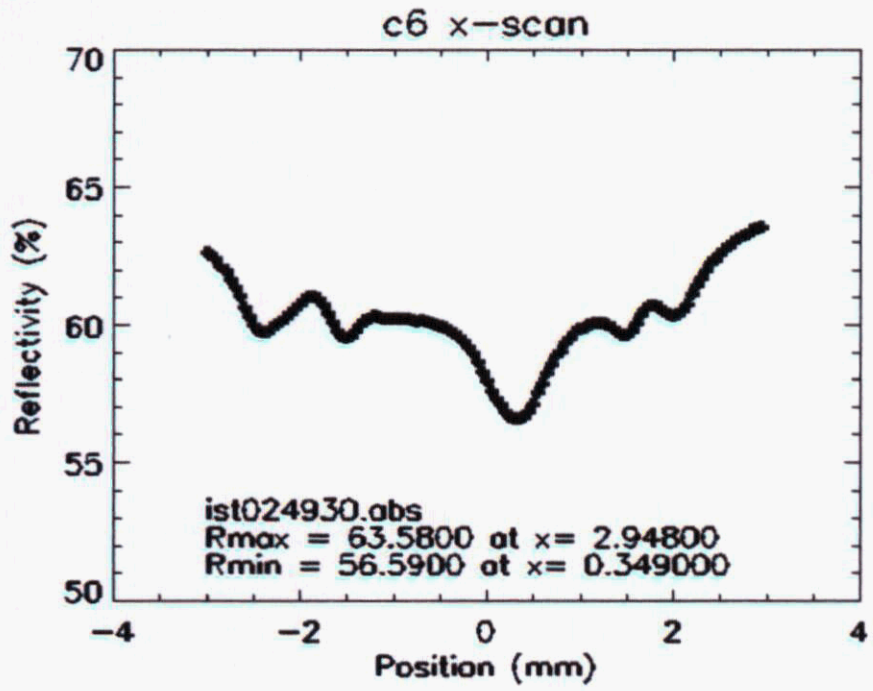

20 bi-layer deep crater

Figure 5

Absolute reflectivity scans made on the calibrated reflectometer beamline 6.3.2 at the ALS for craters of different depth. Note the consistent drop in reflectivity across the repaired region and the additional reflectivity loss due to layer removal for the 15 and 20 bi-layer deep craters.

The drop in reflectivity at the bottom of the crater can be attributed to layer removal and is visible in both the high-resolution measurements, Figure 4, and calibrated reflectivity measurements, Figure 5. At the deepest point the crater is 20 bi-layers deep - half the thickness of the 40-bilayer multilayer at which point we expect a reflectivity loss $(\Delta R/R_o)$ of ≈8% from simply removing 20 layers from the original 40 bi-layer stack. In practice the reflectivity drop due to layer removal, as observed in the centre of the crater, will place an upper bound on the depth of defect that can be repaired using this technique. From Figure 4 and Figure 5 we also see that there is noticeable drop in reflectivity across the entire milled area of about of ≈8% $(\Delta R/R_o)$ in the high-resolution scans. Measurements on the BL6.3.2 reflectometry standards beamline at the ALS on craters of different depths shown in Figure 5 confirm that there is a consistent drop in reflectivity of ≈4% in the milled region. The cause of this is not precisely known at this stage, however this ≈4% average degradation in reflectivity is consistent with the known reflectivity drop attributable to

oxidation of the exposed Mo layers, and we tentatively suggest that this is the cause of the observed decrease in reflectivity across the repaired region.

To this end we are investigating the local application of passivating capping layers to the repaired region using in-situ ion beam sputtering, illustrated in Figure 6, to inhibit oxidation of the exposed Mo layers. First the craters are milled using a 500eV Ar ion beam as described above. A capping layer is locally applied to the repaired region by directing the same ion beam onto a small sputter target, in this case Silicon, located near the repair site, depositing a thin layer of capping material on the repaired region and little material elsewhere. Note, however, that the capping layer crosses alternate layers and thickness' of Mo and Si as the upper layers of the multilayer stack, and if the capping material has a high cross-section in the EUV interference effects between EUV reflected from the multilayer and the capping layer cause in variations in reflectivity. Selection of the right material and thickness for the capping layer is therefore essential in order to control reflectivity variations across the repaired region. Multilayer calculations indicate that the reflectivity variation across the crater can be reduced to 1.5% or less and achieving this in practice is currently the subject of ongoing research.

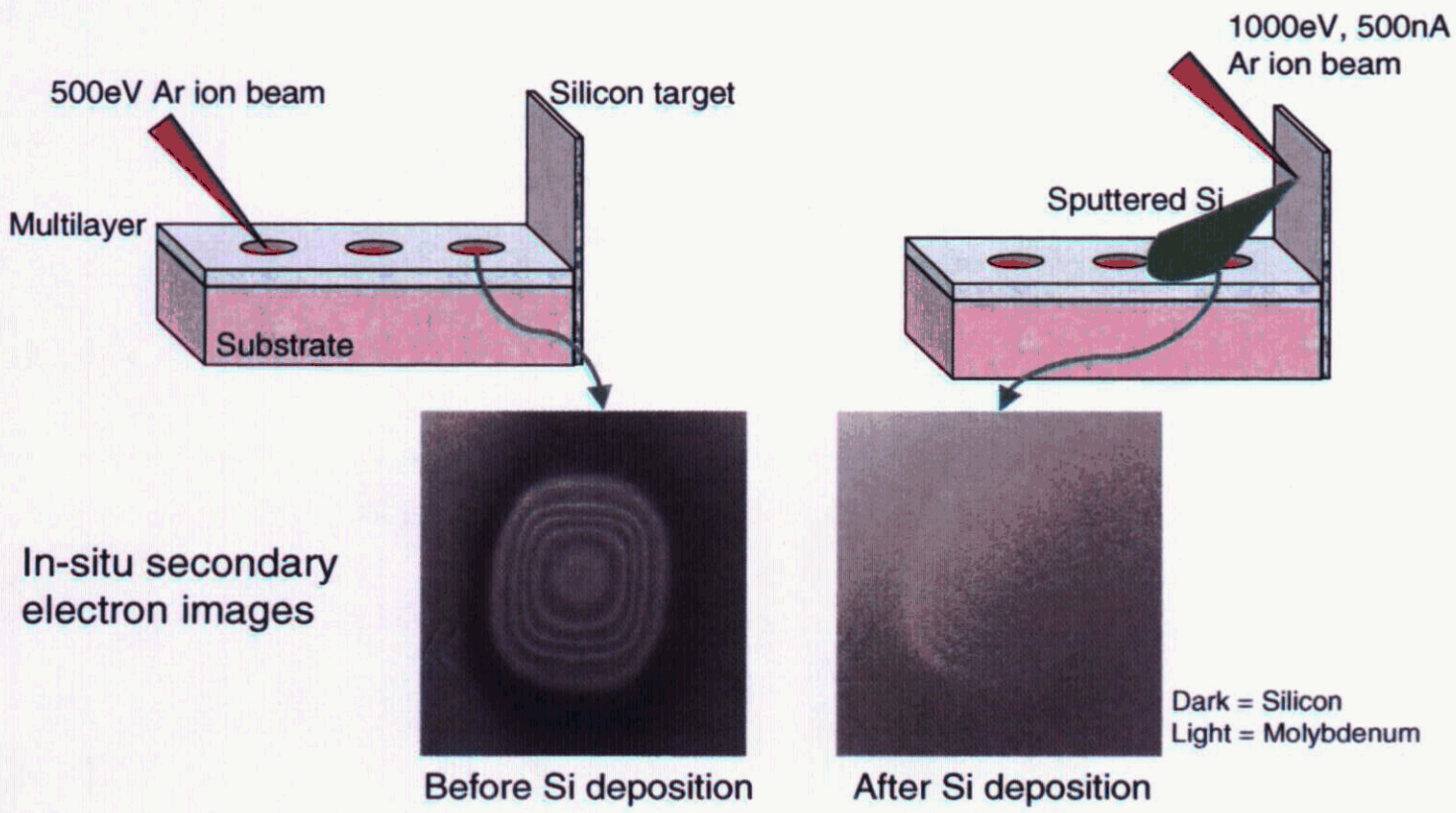

Figure 6
In-situ ion beam sputtering is used to apply a localised capping layer to the repaired region.

3 Phase defect repair

We have also developed techniques for the repair of defects nucleated in the base of the multilayer stack. This process, the basis of which has been described elsewhere[5], uses localised heating of the multilayer by an electron beam to induce a contraction throughout the bulk of the multilayer as shown in Figure 7. The elevated temperature in the region of the beam activates interdiffusion of the Mo/Si layers leading to growth of a silicide layer at the Mo/Si interfaces, a process that causes local contraction of the multilayer period in the heated region due to the difference in density between the silicide and the Mo and Si required to form the silicide. An electron beam penetrates the multilayer allowing the contraction to be distributed through a significant thickness of the multilayer, which is typically 40 or more bi-layers thick. By spreading out the contraction over a large number of layers a relatively large displacement in the top layers (of the order of nm) can be induced with a relatively small contraction of the individual layer period and, thus, comparatively little shift in the peak reflectivity wavelength of the multilayer

---

[5] P.Mirkarimi, D.Stearns, S.Baker, J.Elmer, D.Sweeney and E.Gullikson: "Method for repairing Mo/Si multilayer thin film phase defects in reticles for extreme ultraviolet lithography" (2002) **91(1)** J.Appl.Phys. 81

To effectively model this repair process we used Mote-Carlo modeling to calculate the energy deposition profiles for electron beams of various energies[6], and the calculated energy deposition profile of 10 and 16keV electrons in an 80 bilayer Mo/Si multilayer stack on a ULE substrate is illustrated in Figure 7. This energy deposition profile is used to calculate the expected temperature distribution in the multilayer using finite element modeling and, hence, the expected silicide growth rate[7]. The layer contraction calculated from the silicide growth is then applied to data on the layer structure formed as the multilayer grows over a defect to accurately model the repair of a phase defect. The results of the calculations are shown in Figure 8. The modeled electron energy deposition profile of a 10kV electron beam with a current of 5.3μA into a 100nm FWHM Gaussian spot was applied for 900ms to the layer structure that results from depositing an 80-bilayer pair Mo/Si multilayer on a 100nm spherical particle under optimum smoothing conditions. The layer structure before repair is shown in the upper left and the top layers after repair are shown on the upper right. The line sections below are the resulting profiles at the top, 7th and 15th layers of the repaired region that corresponding to a repair that gives a flat phase for the reflected field.

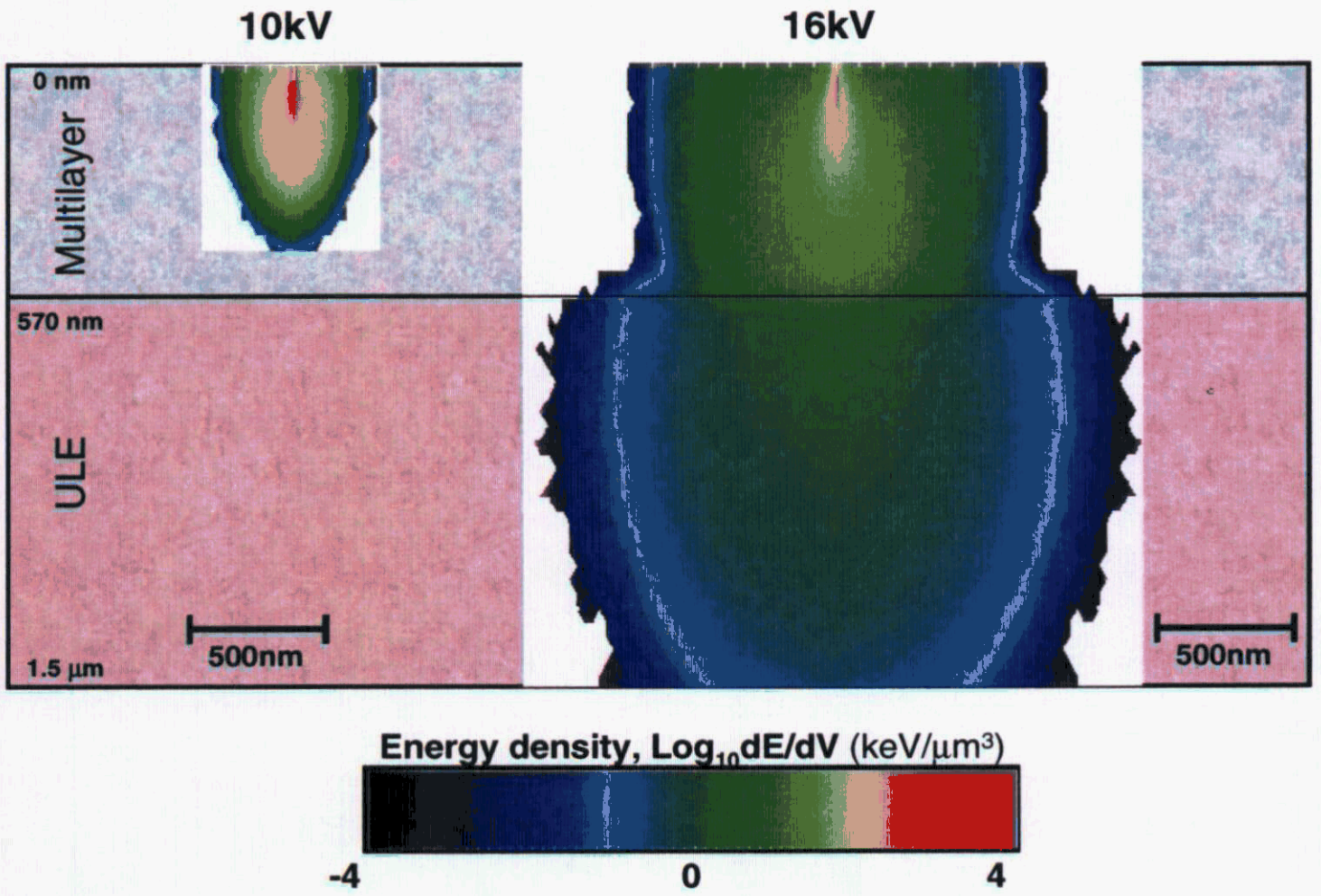

Figure 7

Energy deposition profiles for 10 and 16 kV electrons into a 80 bilayer Mo/Si multilayer on a ULE substrate. The repair of phase defects involves locally heating the multilayer wit a focussed source such as an electron beam. The multilayer heating induces silicide growth at the Mo/Si interfaces to cause local contraction of the multilayer, the extent of which can be controlled through the electron dose so as to smooth out the phase effect of the defect as shown in Figure 8 below.

---

[6] Energy deposition profiles were obtained from Motorola [Scott Hector, Jonathan Cobb, Vladimir Ivin, Mikhail V. Silakov, and George A. Babushkin, "Bremsstrahlung Emission and Absorption in Electron Projection Lithography," *Emerging Lithographic Technologies V*, *SPIE Proceedings* volume 4343, 95-106.] and Sergey Babin of Soft Services, and they were also calculated independently at LLNL for the purposes of comparison.

[7] P.Mirkarimi, D.Stearns, S.Baker, J.Elmer, D.Sweeney and E.Gullikson: "Method for repairing Mo/Si multilayer thin film phase defects in reticles for extreme ultraviolet lithography" (2002) **91(1)** J.Appl.Phys. 81

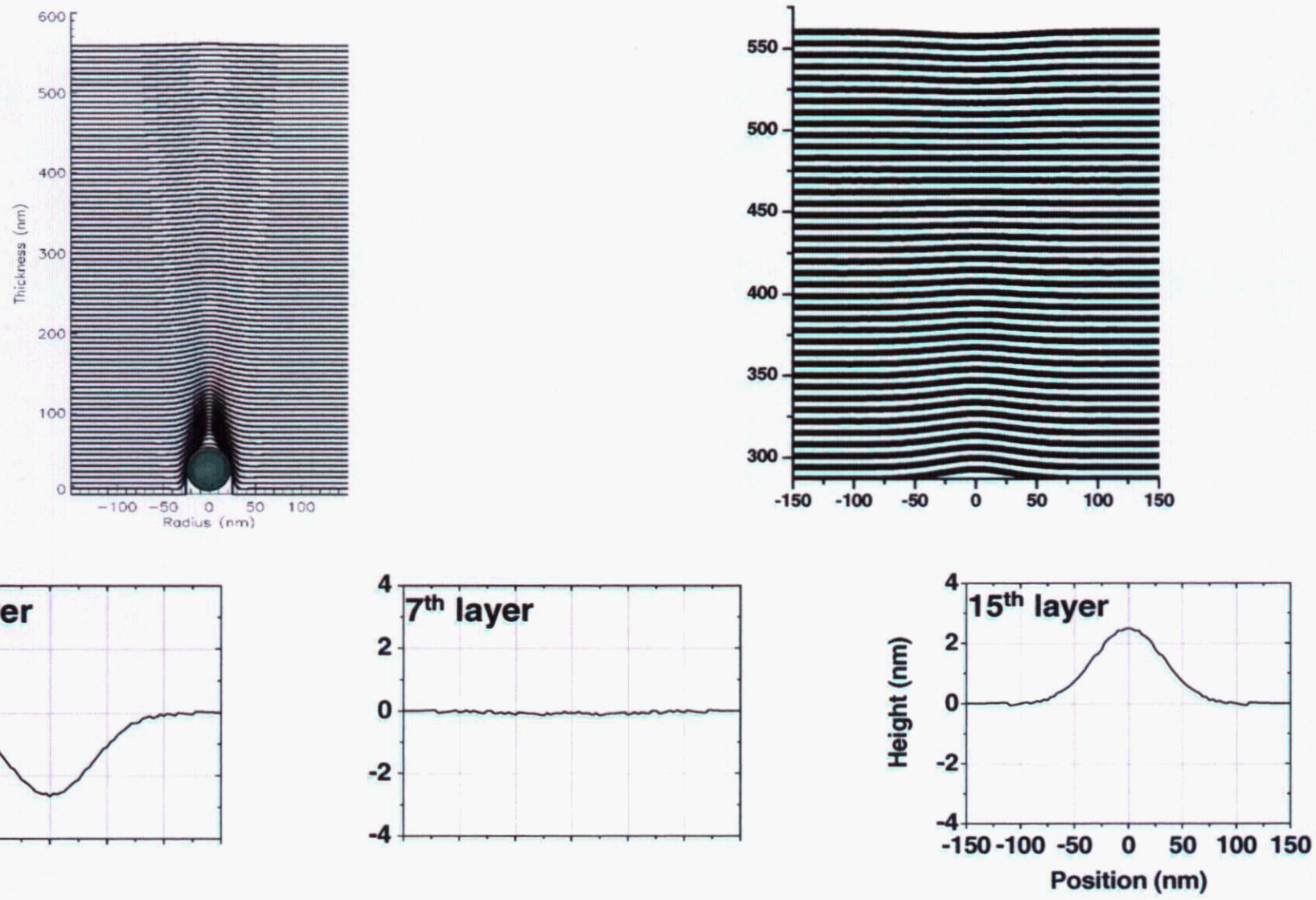

Figure 8

Simulated repair of a phase defect based on the modeled electron energy deposition profile described in the text applied to the layer structure that results from depositing an 80-bilayer pair Mo/Si multilayer on a 50nm spherical particle under optimum smoothing conditions. The layer structure before repair is shown in the upper left and the top layers after repair are shown on the upper right. The line sections below are the resulting profiles at the top, 7th and 15th layers of the repaired region that corresponding to a repair that gives a flat phase for the reflected field.

4 Defect classification and review

We have described two different strategies for repairing phase and amplitude defects nucleated respectively in the bottom or the top layers of the multilayer stack. But in order to successfully apply these distinct repair strategies to mask blank defects it is necessary to have some means of distinguishing between the two. Preliminary calculations indicate that such classification of defect types can be done using a high-resolution actinic mask inspection microscope. Amplitude defects, as the name implies, primarily affect the amplitude of the reflected field and blur symmetrically through focus. Phase defects, on the other hand, display a contrast reversal through focus provided the numerical aperture (NA) of the objective is sufficiently high that the amount of light scattered outside of the objective pupil is negligible. Aerial image simulations illustrating this through-focus effect are shown in Figure 9, inspection of which shows the difference in through-focus behaviour of phase and amplitude defects which can be exploited for defect classification prior to repair. The same microscope could, of course, be used for review of the repair to determine how successful it has been and whether further repair is required, and we are currently in the process of investigating suitable designs for a mask microscope system. Furthermore, a recent study of EUV mask blank cost indicated that the use of the amplitude and phase defect repair combined with defect review using an EUV microscope might allow the target defect density to be relaxed by two to four times.[8]

---

[8] Scott D. Hector, "EUVL Masks: Requirements and Potential Solutions," to be published in *Emerging Lithographic Technologies VI*, *SPIE Proceedings* volume 4688, 2002.

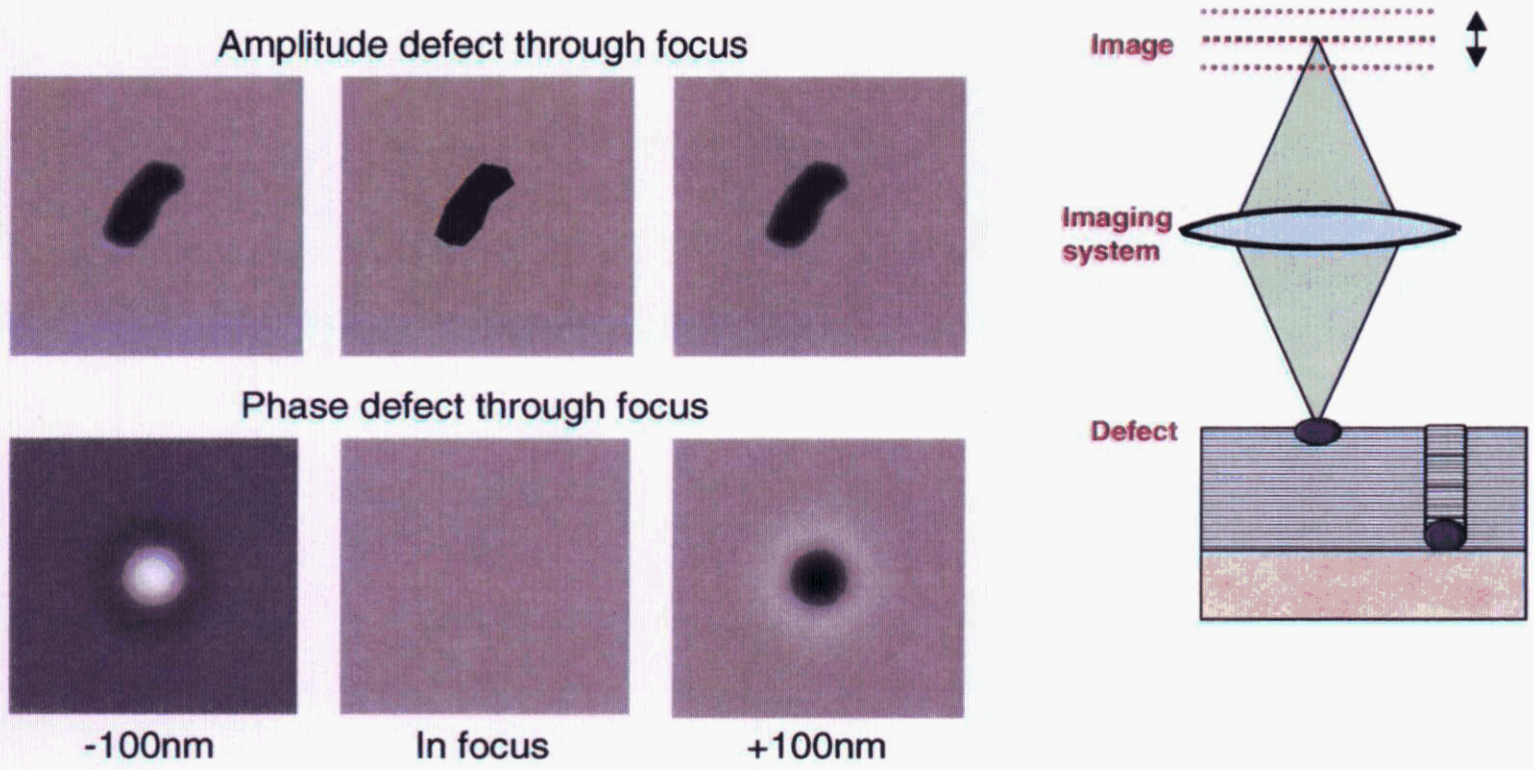

Figure 9

Illustration of the different though-focus behaviour of phase and amplitude defects that can be exploited for defect characterisation.

5 Conclusions

We have presented two different strategies for repairing phase and amplitude defects nucleated respectively in the bottom or the top layers of the multilayer stack. Amplitude defects can be repaired by local removal of the upper layers of the multilayer stack to produce a smooth, shallow and slowly varying crater in the multilayer surface. Properly effected this removes the defective region of the multilayer and substantially restores the multilayer reflectivity in the repaired region and introduces only a small phase shift over the repaired area that will not print within the process window of the printing tool. We have performed preliminary experiments to investigate the feasibility of this technique and have produced craters up to 20 bi-layers deep in Mo/Si multilayers and observed a reflectivity drop in the repaired region which is consistent with layer removal plus an additional amount consistent with the known reflectivity degradation of exposed Mo layers.

We have also further refined the electron beam phase defect repair strategy by incorporating the energy deposition profile of the electron beam into our thermal calculations which has enabled refinement of the tool specifications required for this technique. Strategies for defect classification based on an actinic mask inspection microscope have been developed, and work is currently in progress to investigate suitable designs for implementing such an inspection system for EUV reticles.

ACKNOWLEDGEMENTS

The authors wish to thank Eric Gullikson for access to beamline 6.3.2 at the ALS.

This work was performed under the auspices of the US Department of Energy by the University of California, Lawrence Livermore National Laboratory under contract No. W-7405-Eng-48. Funding was provided by the Extreme Ultraviolet Limited Liability Company (EUV LLC) under a Cooperative Research and Development Agreement.